PHOTONICS Research

Spectrally programmable Raman fiber laser with adaptive wavefront shaping

Yanli Zhang,[1,†] Shanshan Wang,[1,†] Mingzhu She,[1] Yunjiang Rao,[1,2] and Weili Zhang[1,3]

[1]Fiber Optics Research Centre, School of Information and Communication Engineering, University of Electronic Science and Technology of China, Chengdu 611731, China
[2]e-mail: yjrao@uestc.edu.cn
[3]e-mail: wl_zhang@uestc.edu.cn

Received 19 August 2022; revised 23 October 2022; accepted 24 October 2022; posted 26 October 2022 (Doc. ID 473609); published 14 December 2022

Raman fiber lasers (RFLs) have broadband tunability due to cascaded stimulated Raman scattering, providing extensive degrees of freedom for spectral manipulation. However, the spectral diversity of RFLs depends mainly on the wavelength flexibility of the pump, which limits the application of RFLs. Here, a spectrally programmable RFL is developed based on two-dimensional spatial-to-spectral mapping of light in multimode fibers (MMFs). Using an intracavity wavefront shaping method combined with genetic algorithm optimization, we launch light with a selected wavelength(s) at MMF output into the active part of the laser for amplification. In contrast, the light of undesired wavelengths is blocked. We demonstrate spectral shaping of the high-order RFL, including a continuously tunable single wavelength and multiple wavelengths with a designed spectral shape. Due to the simultaneous control of different wavelength regions, each order of Raman Stokes light allows flexible and independent spectral manipulation. Our research exploits light manipulation in a fiber platform with multi-eigenmodes and nonlinear gain, mapping spatial control to the spectral domain and extending linear light control in MMFs to active light emission, which is of great significance for applications of RFLs in optical imaging, sensing, and spectroscopy.

https://doi.org/10.1364/PRJ.473609

1. INTRODUCTION

The rise of multi-dimensional light control in recent years provides a competitive tool for modulating normal and complex lasing in the spatial, spectral, and temporal domains and for studying nonlinear interactions and dynamics in fiber laser systems, e.g., stimulated Raman scattering (SRS), four-wave mixing [1], spatiotemporal control of pulses [2], and multi-dimensional control of multimode fiber (MMF) lasers [3].

The ability to manipulate active emission of light at any desired wavelength has a huge potential in diverse areas. Fiber lasers with wide wavelength tunability [4,5], multiple wavelengths [6,7], high spectral purity [8,9], and arbitrary spectral shapes are under rapid development, and proof-of-concept applications in wavelength selective illumination [10], multi-color imaging [11], super-resolution spectroscopy [12], optical computing [13], and hyperspectral remote sensing [14] have been demonstrated. Generally, the gain of fiber lasers is provided by rare-earth-doped fibers, stimulated Brillouin scattering, or SRS, and the feedback is provided by fiber Bragg gratings or fiber loops with filters, which collectively determine the spectral characteristics of output. Taking advantage of cascaded SRS and distributed Rayleigh scattering [15–17], Raman fiber lasers (RFLs) can lase at arbitrary wavelengths across the fiber transparency window, breaking the limitation of specific emission wavelength regions of active fibers (e.g., ytterbium-doped fiber and erbium-doped fiber). Continuous wavelength tuning of the high-order RFL from 1 to 1.9 μm has been reported by adjusting the wavelength and power of the pump [18,19], confirming the wavelength tunability of RFLs in ultra-wideband. However, the lasing wavelength of high-order RFLs depends mainly on the pump wavelength, and the lasing spectrum of higher Raman Stokes order cannot be freely designed. Active spectral shaping that allows simultaneous spectral manipulation of different Raman Stokes orders is of great importance but remains underdeveloped.

A promising solution to this problem is introducing a programmable filter into RFLs. There are two methods to realize this filter using spatial light modulators (SLMs). Method 1 is to combine an SLM and diffraction grating [20]. Light is first dispersed into different spectral components by the grating and illuminates onto the SLM, which feeds back the target spectral components by selectively activating individual spatial elements. It is a one-dimensional spectral-to-spatial mapping with limited and contradictory bandwidth precision and wavelength range determined by the size and number of pixels of SLMs.

Method 2 is to combine an SLM and scattering medium [21–25]. Due to the interference among the eigenmodes of the scattering medium, wavelength-sensitive speckle patterns are formed at the output, providing a spectral correlation bandwidth (SCB) for filtering. This deterministic coupling of spatial and spectral degrees of freedom in scattering media allows spectral control using wavefront shaping (WFS) [26]. Compared with conventional gratings, scattering media can achieve two-dimensional spatial-to-spectral mapping with a finer filtering bandwidth and remarkably extended wavelength range. The limitation is that the minimum bandwidth is inversely related to the thickness of the scattering media, which leads to a significant optical loss and is not compatible with fiber systems.

Interestingly, MMFs can serve as a particular scattering medium due to strong intermodal interference. Benefiting from its waveguide structure, MMFs exhibit good optical confinement and minimal loss, providing a fascinating platform for light transmission and manipulation [27–29]. Various functional devices have been developed based on the scattering characteristics of MMFs, such as spectrometers [30,31], endoscopes [32,33], and optical sensors [34]. Especially, multi-dimensional control of MMF lasers is flourishing [3,35,36]. There is no doubt that MMF-based fiber systems have the potential to simultaneously control Raman lasing of different orders without the limitations mentioned above, which have not yet been investigated.

In this work, we propose a spectrally programmable RFL based on spatial-to-spectral mapping of light in MMFs, where the spectral degrees of freedom of the RFL are well harnessed. Spectral shaping is achieved by combining an MMF and SLM, which focuses the light with a target wavelength(s) into the active part of the laser using adaptive WFS. We demonstrate independent and flexible spectral shaping from the first to third order of Raman Stokes emission via automatic optimization of the filtering effect and adjustment of the pump power, providing a powerful light source for future optical information applications.

2. PRINCIPLE AND EXPERIMENTAL SETUP

A. Spectral Correlation of Speckle in MMFs

As monochromatic light propagates in a large-core MMF, a unique speckle pattern is generated at the MMF output end due to multi-mode interference [10]. Moreover, wavelength-shifted light experiences a slightly modified propagation constant in the MMF, resulting in a significant change in phase delay and altering the speckle pattern. The wavelength sensitivity, i.e., the aforementioned SCB, depends mainly on the structural parameters of the MMF, including the length, numerical aperture, and core diameter [30]. To simplify the analysis, we express the electric field at the output end of an MMF as

$$E(r,\phi,\lambda,z)=\sum_{n=1}^{N}A_n e_n(r,\phi,\lambda)e^{-i[\beta_n(\lambda)z-\omega t+\varphi_n]}, \quad (1)$$

where e_n and β_n are the spatial profile and propagation constant of the nth guided mode, respectively, calculated by solving Maxwell's equations [37]. A_n and φ_n are the amplitude and initial phase of the mode, respectively. It is assumed that all modes are excited equally, with initial phases randomly distributed between zero and 2π. Light with different wavelengths creates distinct speckle patterns at the output due to the superposition of guided modes with respective accumulated phases. Considering 300 guided modes in a step-index MMF with a core diameter of 105 μm, we numerically simulated the effect of fiber length on the SCB. The speckles inside the white circles in Fig. 1(a) show the process of speckle decorrelation of a 1.5 m long MMF when the wavelength varies by 0.1 nm. The spectral correlation function, defined as $C(\Delta\lambda)=\langle\langle I(x,\lambda)I(x,\lambda+\Delta\lambda)\rangle_\lambda/[\langle I(x,\lambda)\rangle_\lambda\langle I(x,\lambda+\Delta\lambda)\rangle_\lambda]-1\rangle_x$, explains the degree of correlation of the speckle patterns as the wavelength changes, where $I(x,\lambda)$ is the intensity of wavelength λ at position x, $\Delta\lambda$ is the change in wavelength, and $\langle\cdots\rangle_\lambda$ represents averaging over the spectral domain. Spectral correlation functions corresponding to different lengths of MMFs are calculated numerically in Fig. 1(b). We can then extract the half-width at half maximum (HWHM) of these curves. The related values of SCB, $\Delta\lambda_C$ (i.e., twice the HWHM), are plotted in Fig. 1(c), reflecting the decrease of SCB with increasing MMF length.

Similarly, $C(\Delta\lambda)$ and $\Delta\lambda_C$ are measured experimentally using a tunable laser and a near-infrared camera. The results are given in Figs. 1(d) and 1(e) by collecting speckle patterns at wavelengths from 1549.5 to 1550.5 nm, showing good accordance with the numerical results. Light with wavelengths beyond the SCB can be mapped one to one to uncorrelated speckle patterns, which allows us to develop a filter by WFS. Here the length of the MMF is considered mainly as a parameter that determines the bandwidth precision of the filter.

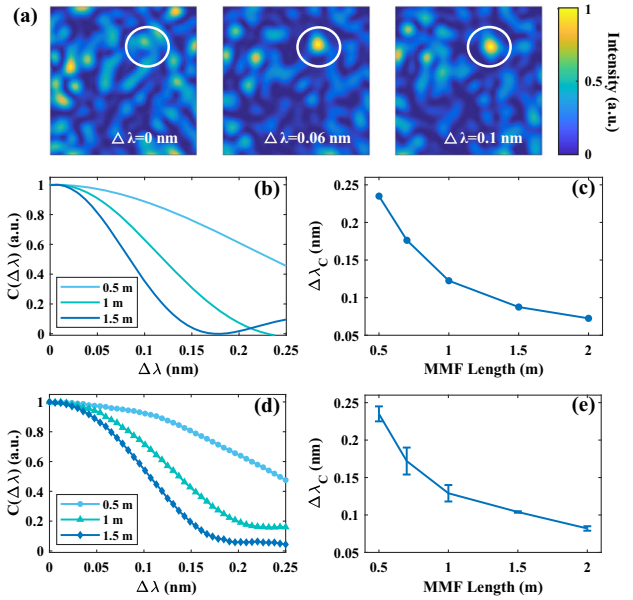

Fig. 1. Wavelength-sensitive characteristic of the MMF. (a) Normalized speckle patterns at different input wavelengths for an MMF length of 1.5 m. (b) Simulated and (d) measured spectral correlation functions versus wavelength change for different lengths of MMF. (c) Simulated and (e) measured spectral correlation bandwidths for MMFs with different lengths.

B. Working Mechanism and Experimental Setup

The RFL consists of a filter and an active part, and its working mechanism and experimental setup are depicted in Fig. 2. The filter acts as a wavelength programmable point reflector that selectively feeds the spontaneous Raman scattered light as seed light to control the cascaded Raman Stokes emission. Light from the active part is first coupled into a segment of step-index MMF with core/cladding diameters of 105/125 μm and a numerical aperture of 0.22, collimated by lens 1 (L1, Thorlabs, C171TMD-C, effective focal length 6.2 mm) and expanded by a beam expander (L2, L3, 10×, Thorlabs, GBE10-C). It is then polarized and illuminates onto a phase-only SLM (Meadowlark Optics, 1920 × 1152 pixels), which is high-power tolerant and shapes the phase front of input light, and the modulated light is fed back into the MMF. The single-mode fiber (SMF) of the active part is spliced with the MMF. Due to the mode field mismatch between the MMF and SMF, the spectral profile of the feedback into the active part is determined by the portion of the speckle pattern coupled to the SMF (i.e., the mode field overlap) at the MMF–SMF splicing point [38]. Thus, the filter operates by modulating the wavelength-sensitive speckle patterns of the MMF with SLM-controlled WFS. Once the light of the desired wavelength(s) is focused at the MMF–SMF splicing point, more light energy is injected into the active part of the RFL for amplification, hence manipulating the lasing spectrum.

The active part combined with the filter part constitutes a spectrally programmable RFL with a forward-pumped half-opened cavity structure [39]. An ytterbium-doped random fiber laser (YRFL) is first achieved, which is directly pumped by a 976 nm laser diode (LD) through a wavelength-dependent signal-pump combiner. The feedback is provided by a 1090 nm high-reflectivity fiber Bragg grating and distributed Rayleigh scattering in a 15 km long SMF. Cascaded Raman lasing can be realized based on the YRFL pump and the reflective filter, where the SMF provides both Raman gain and distributed Rayleigh scattering feedback. A wideband wavelength division multiplexer (port 1: 1070–1090 nm, port 2: 1100–1700 nm) is used to separate the feedback of the YRFL and RFL corresponding to different wavelength bands.

Spectral shaping is implemented via iterative optimization of a noise-resistant genetic algorithm (GA) [40], in which the fitness function and parameters are optimized as needed. We evenly divide the SLM into 44 × 44 macropixels for better mode matching with the MMF and improved coupling efficiency. Each macropixel is a block of 25 × 25 pixels, and the phase is controlled independently between zero and 2π. To balance convergence rate and fitness value enhancement, we take a set of 60 random phase maps as an initial population, which eventually converge to an optimized pattern to strengthen the desired spectral features. The pump source is required to be online during the optimization process, and the security of

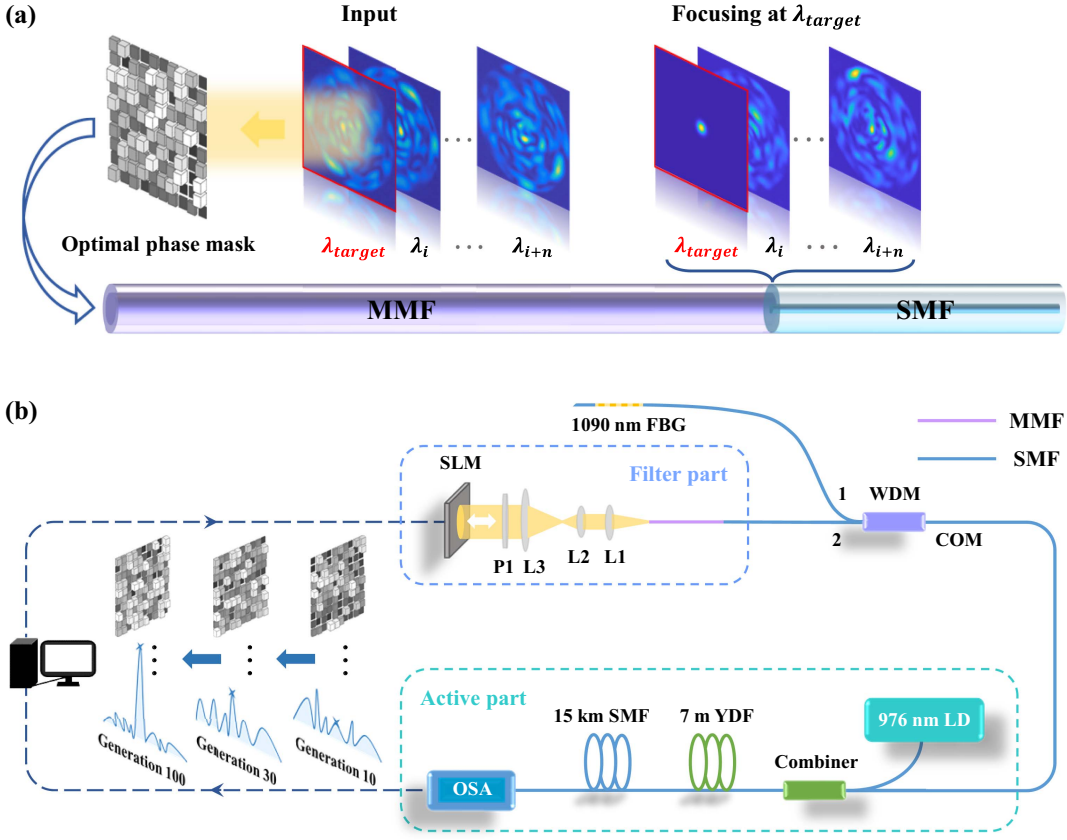

Fig. 2. Working mechanism and experimental setup of the spectrally programmable Raman fiber laser. (a) Working mechanism and (b) schematic diagram. FBG, fiber Bragg grating; WDM, wavelength division multiplexer; Combiner, signal-pump combiner; LD, laser diode; YDF, ytterbium-doped fiber; SLM, spatial light modulator; P1, polarizer; L1, L2, L3, lens; SMF, single-mode fiber; MMF, multimode fiber; OSA, optical spectrum analyzer. The inset shows the optimization process.

the laser system is ensured since only weak backward Raman light is modulated in the free space between the SLM and MMF. An optical spectrum analyzer (OSA, Anritsu MS9710C) with a resolution of 0.05 nm monitors the lasing spectrum, and the intensity value of the wavelength(s) of interest contributes to the fitness function to update the phase pattern of the SLM. The algorithm generates new offspring with higher fitness values by selecting parents, breeding, and mutation operations in each iteration.

By genetic iterations, light with the target wavelength(s) is fed back to the active part while blocking unwanted light as much as possible [see the inserted speckle patterns at the MMF–SMF splicing point in Fig. 2(a)]. Because the feedback acts as the seed light that ultimately determines the lasing spectrum, only a small power of feedback that dominates spontaneous emission is sufficient to control the lasing wavelength, as verified in previous works [15,41]. Once the optimal phase pattern is found, it can be recorded and reloaded to shape the desired spectrum as long as the MMF remains undisturbed. In addition, real-time optimization is performed by monitoring the spectrum as feedback during laser operation to balance the unfavorable effects of slow degradation of the MMF state (keeping the laser running stable and robust to disturbances) [42].

3. RESULTS AND DISCUSSION

A. Performance of the Filter

We first investigate the performance of the reflective filter. A circulator is employed to measure the filtered spectrum, with port 1 connected to a broadband amplified spontaneous emission source, port 2 to the filter, and port 3 to an OSA. The performance of the filter is modulated by the phase pattern loaded onto the SLM. We present an example of single-wavelength filtering by monitoring the intensity value at 1555.5 nm as a fitness function. The spectra before and after optimization are given in Fig. 3(a), where the length of the MMF is 1 m. The unoptimized spectrum is noisy and disordered due to the randomness of the wavelength-sensitive speckle patterns. In contrast, the optimized output spectrum establishes a peak at the target wavelength with a peak-to-ground ratio of 13 dB. Figure 3(b) shows the corresponding optimization process, where the fitness value grows with iterations and eventually converges after 800 generations. As verified in the previous section, the length of the MMF determines the SCB, which is available to set the bandwidth precision of the filter. We also record optimized filtered spectra using MMFs with different lengths. The inset of Fig. 3(a) reveals that the measured minimal 3 dB bandwidth of the filtering decreases as the MMF length increases, which matches well with the conclusion of Fig. 1.

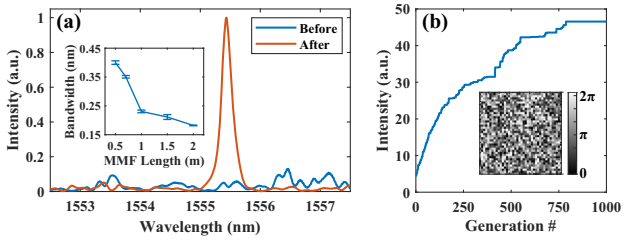

Fig. 3. Performance of the filter. (a) Spectra before and after optimization. The optimized wavelength is 1555.5 nm. The inset shows the filtering bandwidth as a function of MMF length. (b) Optimization process corresponding to (a). The inset shows the optimal phase pattern.

B. First-Order RFL for Single- and Multi-Wavelength Lasing

A spectrally programmable high-order RFL can be obtained by combining the filter and active parts. The wide reflection band of the filter part and the cascaded SRS effect in the active part jointly enable spectral control with high degrees of freedom. Although using a longer MMF means finer spectral control, environmental perturbations lead to a more unstable state of the long MMF, disrupting the optimization process. For trade-offs, we use an MMF with a fixed length of 0.65 m in the following demonstrations.

A continuously tunable single-wavelength RFL is first demonstrated in the first-order Raman Stokes band. Figure 4(a) gives several typical spectra with emission wavelengths from 1138 to 1152 nm in a tuning range of 14 nm, which are plotted on a linear scale and normalized by min-max scaling. The MMF-length-determined bandwidth of single-wavelength lasing is about 0.4 nm, and the optical signal-to-noise ratio is greater than 30 dB, indicating high spectral purity (also known as the in-band power ratio). The output power of the first-order RFL at 1145 nm versus the LD pump power is shown in Fig. 4(b), which indicates that the first-order Raman lasing threshold is 3.8 W, and the conversion efficiency is about 11%. The efficiency can be improved remarkably at the expense of increasing the lasing threshold if a shorter length of SMF is employed in the active part.

Moreover, multi-wavelength lasing with designed wavelength numbers, wavelength positions, and power distribution is realized using a multi-objective GA [43]. Two examples are displayed in Figs. 4(c) and 4(d) for dual- and five-wavelength lasing, respectively, with designed spectral shapes. In our case,

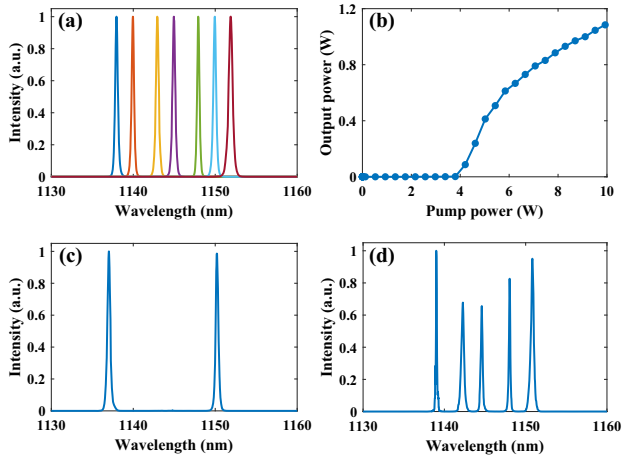

Fig. 4. Output characteristics of first-order RFL. (a) Tunable single-wavelength output. (b) Output power of Raman lasing versus 976 nm LD pump power. (c) Dual-wavelength and (d) five-wavelength output.

the optical signal-to-noise ratio degrades with the increasing number of controlled wavelengths. It can be promoted by increasing the number of macropixels and the free-space coupling efficiency of modulated light. Completely different from filters based on Fabry–Perot cavities or SMF–MMF–SMF structures, where the spectral shape cannot be designed freely, this customized spectral shape verifies the good flexibility to control laser emission in the spectral domain.

C. High-Order RFL for Cascaded Spectral Manipulation

Existing filters cannot cover a broad band while maintaining relatively high bandwidth precision. Therefore, broadband wavelength tuning of high-order RFLs can be achieved only by adjusting the pump wavelength with restricted control over spectral shape and bandwidth unless multiple filters of different wavelength bands are used together. Our proposed high-order RFL can overcome these limitations. Using adaptive intracavity WFS, the wavelength interval of different orders of Raman Stokes light can be freely designed, which greatly broadens the spectral manipulation range of higher Raman order.

The performance of the spectrally programmable high-order RFL is presented in Fig. 5 as a further functional demonstration of the proposed laser. To control the lasing wavelength of different Raman Stokes orders, we optimize the spectrum in several stages according to the cascaded order. The final phase pattern in the previous stage is taken as the starting point for optimizing the higher-order Raman lasing. Figures 5(a) and 5(b) show tunable single-wavelength lasing in the second- and third-order Stokes bands, respectively, while keeping the lower-order wavelength constant. In Fig. 5(a), we first optimize the first-order wavelength to 1143 nm (inset) at a pump power of 8.5 W, i.e., the first stage. Then, the pump power is increased to 14.5 W to achieve second-order Raman lasing, and spectra with central wavelengths of 1202.1, 1206.4, and 1210.6 nm are obtained after further optimization, i.e., the second stage. Similarly, the third-order RFL in Fig. 5(b) can be tuned by a three-stage optimization, wherein the first two stages optimize the first- and second-order wavelengths to 1143 and 1211 nm, respectively (inset), and the third stage optimizes the third-order Raman lasing at wavelengths of 1276.7, 1280.6, and 1286.5 nm.

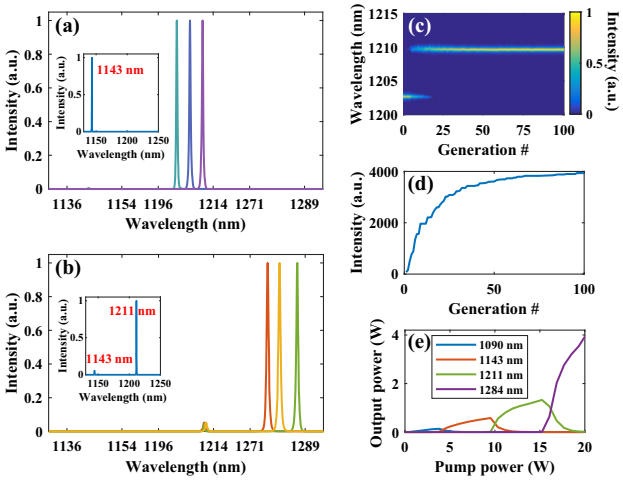

Fig. 5. Output characteristics of high-order RFL. (a) Wavelength tunability of the second-order RFL. The inset is the corresponding first-order Raman lasing spectrum. (b) Wavelength tunability of the third-order RFL. The inset shows the corresponding lower-order Raman lasing spectrum. (c) Evolution of wavelength switching from 1203 to 1210 nm for the second-order RFL. (d) Intensity value enhancement at the wavelength of 1210 nm corresponding to (c). (e) Output power of the high-order RFL versus 976 nm LD pump power.

The running RFL can also switch the lasing wavelength dynamically. Figures 5(c) and 5(d) show the process of wavelength switching from 1203 to 1210 nm after 100 genetic iterations. Once the laser emission is on, the algorithm of wavelength switching can converge faster, typically taking about 10 min. The time consumption is determined mainly by the running speed of the SLM and the OSA. In our case, the SLM frame rate is 31 Hz, and the speed of data acquisition of the OSA limits the iteration speed of optimization. A digital micromirror device with a kHz frame rate can replace the SLM for WFS. Moreover, optimization time can be significantly reduced using an advanced spectrometer combined with field-programmable gate array processing. Taking single-wavelength lasing at 1143, 1211, and 1284 nm as an example, Fig. 5(e) shows that the output power transfers between the lower-order and higher-order Raman lasing. The lasing efficiency increases with the emission order since the optimization is performed order by order. Due to the direct and real-time control of each Stokes order, there is only a slight nonlinear broadening of the emission bandwidth with increasing pump power.

D. Output Characteristics of the Spectrally Programmable RFL

Furthermore, we measure the output characteristics of the spectrally programmable RFL, including spectral purity, operating wavelength range, and output stability. Spectral purity is determined by the percentage of total output power in the desired Stokes wavelength band due to cascaded SRS. The spectral purity of single-wavelength emission for different Raman Stokes orders is shown in Fig. 6(a) when the pump power is set to 9, 15, and 20 W. Due to the robust spectral manipulation capability brought by intracavity WFS, the RFL has high spectral purity for each Stokes order.

Considering the free-space coupling loss caused by misalignment and the zeroth-order diffraction efficiency of the SLM (~80%), we measure the reflectivity of the programmable filter, which is about 18.4% for a single wavelength. The whole gain bandwidth of the higher Stokes order is determined by the Raman gain spectrum and the wavelength tuning range of the previous order. In our case, the achievable reflectivity of the filter directly determines the tuning range of the first-order Raman lasing. While the tuning range of higher orders can be considerably increased because both the emission light and its pump light can be tuned independently, we realize a 29.5 nm tuning range (from 1192.8 to 1222.3 nm) for the second-order RFL, as depicted in Fig. 6(b), which is more than twice that of the first-order RFL.

The proposed target-oriented laser allows adaptive optimization to overcome the performance degradation due to the

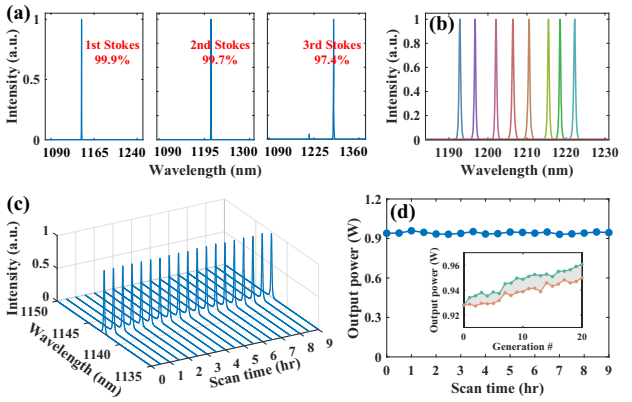

Fig. 6. Output characteristics of the spectrally programmable RFL. (a) Optimized lasing spectra and spectral purity for each Stokes order. The pump powers corresponding to the first-, second-, and third-order Raman lasing spectra are 9, 15, and 20 W, respectively. (b) Wavelength tunability of second-order RFL at a fixed pump power of 9 W. (c) Spectral stability of single-wavelength lasing at 1142.5 nm. (d) Output power stability corresponding to (c). The inset shows the output power fluctuations in one optimization period.

time-dependent variation of the MMF's transmission matrix in unstable environments (e.g., mechanical disturbance or temperature changes). The spectrum is optimized in real time by setting a start and stop threshold for the target wavelength. Once the intensity value falls below the start threshold, the GA re-runs based on the current phase pattern until the intensity value exceeds the stop threshold. It should be noted that the crossover and mutation operations of the GA generate new individuals causing spectral and output power instability during the optimization process. To avoid performance fluctuations, we set the mutation rate to 0.15% (i.e., only three of the macropixels are mutated for a phase pattern). In addition, we consider a moderate MMF length in the laser system to mitigate the degradation of the MMF transmission matrix over time. Taking the single-wavelength lasing of the first-order RFL at a fixed pump power of 9 W as an example, we test the output stability at the target wavelength of 1142.5 nm over 9 h, including the spectral and output power stability, as shown in Figs. 6(c) and 6(d). The maximum spectral peak fluctuation is 3.6%, and the maximum output power fluctuation is 2.8%, demonstrating the high stability and utility of the proposed laser. The subplot in Fig. 6(d) shows that the power variations in one optimization period are less than 1.5%. The green and orange dots indicate the maximum and minimum power values in each generation, respectively.

4. CONCLUSION

In conclusion, we proposed a spectrally programmable RFL based on SLM-controlled wavelength-sensitive spatial focusing of light. The laser consists of a reflective filter part dominated by spatial-to-spectral mapping in the MMF–SMF structure and an active part providing Raman gain and distributed Rayleigh scattering feedback, allowing laser emission at the desired wavelength(s) in the cascaded Raman Stokes band. We demonstrated versatile spectral manipulations of the high-order RFL, including tunable single-wavelength lasing, multi-wavelength lasing with customized spectral shape, real-time wavelength switching, and independent wavelength control of cascaded Raman Stokes light, which has not been reported before, to our knowledge. Moreover, the proposed method potentially broadens the controllable spectral range since the spectrum of different orders of Raman lasing can be shaped flexibly. Further developments will focus on enhancing the reflection efficiency of the programmable filter, extending the wavelength tunable range of each Stokes order, and improving the optimization speed of WFS. It is believed that this work will inspire active light control in laser systems and provide a powerful spectrally programmable laser source for optical information applications.

Funding. National Natural Science Foundation of China (11974071, 61635005).

Disclosures. The authors declare no conflicts of interest.

Data Availability. Data underlying the results presented in this paper are not publicly available at this time but may be obtained from the authors upon reasonable request.

†These authors contributed equally to this work.

REFERENCES

1. O. Tzang, A. M. Caravaca-Aguirre, K. Wagner, and R. Piestun, "Adaptive wavefront shaping for controlling nonlinear multimode interactions in optical fibres," Nat. Photonics **12**, 368–374 (2018).
2. M. Mounaix and J. Carpenter, "Control of the temporal and polarization response of a multimode fiber," Nat. Commun. **10**, 5085 (2019).
3. X. Wei, J. C. Jing, Y. Shen, and L. V. Wang, "Harnessing a multidimensional fibre laser using genetic wavefront shaping," Light Sci. Appl. **9**, 149 (2020).
4. V. Balaswamy, S. Aparanji, S. Arun, S. Ramachandran, and V. R. Supradeepa, "High-power, widely wavelength tunable, grating-free Raman fiber laser based on filtered feedback," Opt. Lett. **44**, 279–282 (2019).
5. R. Ma, X. Quan, H. Wu, W. C. Gao, D. J. Huang, X. C. Wang, S. X. Xu, D. Y. Fan, and J. Liu, "20 watt-level single transverse mode narrow linewidth and tunable random fiber laser at 1.5 μm band," Opt. Express **30**, 28795–28804 (2022).
6. J. Ye, Y. Zhang, J. Xu, J. Song, T. Yao, H. Xiao, J. Leng, and P. Zhou, "Broadband pumping enabled flat-amplitude multi-wavelength random Raman fiber laser," Opt. Lett. **45**, 1786–1789 (2020).
7. Q. Zhao, L. Pei, J. Zheng, M. Tang, Y. Xie, J. Li, and T. Ning, "Switchable multi-wavelength erbium-doped fiber laser with adjustable wavelength interval," J. Lightwave Technol. **37**, 3784–3790 (2019).
8. J. Dong, L. Zhang, H. Jiang, X. Yang, W. Pan, S. Cui, X. Gu, and Y. Feng, "High order cascaded Raman random fiber laser with high spectral purity," Opt. Express **26**, 5275–5280 (2018).
9. J. Ye, J. Xu, J. Song, Y. Zhang, H. Zhang, H. Xiao, J. Leng, and P. Zhou, "Pump scheme optimization of an incoherently pumped high-power random fiber laser," Photon. Res. **7**, 977–983 (2019).
10. R. Ma, Z. Wang, W. Y. Wang, Y. Zhang, J. Liu, W. L. Zhang, A. S. L. Gomes, and D. Y. Fan, "Wavelength-dependent speckle multiplexing for imaging through opacity," Opt. Laser Eng. **141**, 106567 (2021).
11. S. Boersma, D. Khuperkar, B. M. P. Verhagen, S. Sonneveld, J. B. Grimm, L. D. Lavis, and M. E. Tanenbaum, "Multi-color single-molecule imaging uncovers extensive heterogeneity in mRNA decoding," Cell **178**, 458–472 (2019).

12. A. Boschetti, A. Taschin, P. Bartolini, A. K. Tiwari, L. Pattelli, R. Torre, and D. S. Wiersma, "Spectral super-resolution spectroscopy using a random laser," Nat. Photonics **14**, 177–182 (2020).
13. X. Xu, M. Tan, B. Corcoran, J. Wu, A. Boes, T. G. Nguyen, S. T. Chu, B. E. Little, D. G. Hicks, R. Morandotti, A. Mitchell, and D. J. Moss, "11 TOPS photonic convolutional accelerator for optical neural networks," Nature **589**, 44–51 (2021).
14. Y. Gu, T. Liu, G. Gao, G. Ren, Y. Ma, J. Chanussot, and X. Jia, "Multimodal hyperspectral remote sensing: an overview and perspective," Sci. China Inf. Sci. **64**, 121301 (2021).
15. S. K. Turitsyn, S. A. Babin, A. E. El-Taher, P. Harper, D. V. Churkin, S. I. Kablukov, J. D. Ania-Castañón, V. Karalekas, and E. V. Podivilov, "Random distributed feedback fibre laser," Nat. Photonics **4**, 231–235 (2010).
16. S. K. Turitsyn, S. A. Babin, D. V. Churkin, I. D. Vatnik, M. Nikulin, and E. V. Podivilov, "Random distributed feedback fibre lasers," Phys. Rep. **542**, 133–193 (2014).
17. W. L. Zhang, Y. J. Rao, J. M. Zhu, Z. X. Yang, Z. N. Wang, and X. H. Jia, "Low threshold 2nd-order random lasing of a fiber laser with a half-opened cavity," Opt. Express **20**, 14400–14405 (2012).
18. L. Zhang, J. Dong, and Y. Feng, "High-power and high-order random Raman fiber lasers," IEEE J. Sel. Top. Quant. Electron. **7**, 1400106 (2018).
19. L. Zhang, H. Jiang, X. Yang, W. Pan, and Y. Feng, "Ultra-wide wavelength tuning of a cascaded Raman random fiber laser," Opt. Lett. **41**, 215–218 (2016).
20. H. Yang, P. Wilkinson, B. Robertson, S. Giltrap, O. Snowdon, H. Prudden, and D. Chu, "24 [1 × 12] wavelength selective switches integrated on a single 4k LCoS device," J. Lightwave Technol. **39**, 1033–1039 (2021).
21. F. van Beijnum, E. G. van Putten, A. Lagendijk, and A. P. Mosk, "Frequency bandwidth of light focused through turbid media," Opt. Lett. **36**, 373–375 (2011).
22. E. Small, O. Katz, Y. Guan, and Y. Silberberg, "Spectral control of broadband light through random media by wavefront shaping," Opt. Lett. **37**, 3429–3431 (2012).
23. D. Andreoli, G. Volpe, S. Popoff, O. Katz, S. Grésillon, and S. Gigan, "Deterministic control of broadband light through a multiply scattering medium via the multispectral transmission matrix," Sci. Rep. **5**, 10347 (2015).
24. H. Li, X. Wu, G. Liu, R. V. Vinu, X. Wang, Z. Chen, and J. Pu, "Generation of controllable spectrum in multiple positions from speckle patterns," Opt. Laser Technol. **149**, 107820 (2022).
25. L. Wan, X. Ji, R. K. Singh, Z. Chen, and J. Pu, "Use of scattering layer as a programmable spectrum filter," IEEE J. Quantum Electon. **55**, 6100306 (2019).
26. I. M. Vellekoop, "Feedback-based wavefront shaping," Opt. Express **23**, 12189–12206 (2015).
27. H. Cao and Y. Eliezer, "Harnessing disorder for photonic device applications," Appl. Phys. Rev. **9**, 011309 (2022).
28. W. Xiong, P. Ambichl, Y. Bromberg, B. Redding, S. Rotter, and H. Cao, "Spatiotemporal control of light transmission through a multimode fiber with strong mode coupling," Phys. Rev. Lett. **117**, 053901 (2016).
29. S. Resisi, Y. Viernik, S. M. Popoff, and Y. Bromberg, "Wavefront shaping in multimode fibers by transmission matrix engineering," APL Photon. **5**, 036103 (2020).
30. B. Redding, S. M. Popoff, and H. Cao, "All-fiber spectrometer based on speckle pattern reconstruction," Opt. Express **21**, 6584–6600 (2013).
31. B. Redding, M. Alam, M. Seifert, and H. Cao, "High-resolution and broadband all-fiber spectrometer," Optica **1**, 175–180 (2014).
32. T. Čižmár and K. Dholakia, "Exploiting multimode waveguides for pure fibre-based imaging," Nat. Commun. **3**, 1027 (2012).
33. M. Plöschner, T. Tyc, and T. Čižmár, "Seeing through chaos in multimode fibres," Nat. Photonics **9**, 529–535 (2015).
34. S. Wu, S. Yin, and F. T. S. Yu, "Sensing with fiber specklegrams," Appl. Opt. **30**, 4468–4470 (1991).
35. L. G. Wright, D. N. Christodoulides, and F. W. Wise, "Spatiotemporal mode-locking in multimode fiber lasers," Science **358**, 94–97 (2017).
36. K. Krupa, A. Tonello, A. Barthelemy, T. Mansuryan, V. Couderc, G. Millot, P. Grelu, D. Modotto, S. A. Babin, and S. Wabnitz, "Multimode nonlinear fiber optics, a spatiotemporal avenue," APL Photon. **4**, 110901 (2019).
37. L. G. Wright, Z. M. Ziegler, P. M. Lushnikov, Z. Zhu, M. A. Eftekhar, D. N. Christodoulides, and F. W. Wise, "Multimode nonlinear fiber optics: massively parallel numerical solver, tutorial, and outlook," IEEE J. Sel. Top. Quantum Electron. **24**, 5100516 (2018).
38. Q. Wang, G. Farrell, and W. Yan, "Investigation on single-mode-multimode single-mode fiber structure," J. Lightwave Technol. **26**, 512–519 (2008).
39. H. Wu, Z. Wang, Q. He, W. Sun, and Y. Rao, "Common-cavity ytterbium/Raman random distributed feedback fiber laser," Laser Phys. Lett. **14**, 065101 (2017).
40. D. B. Conkey, A. N. Brown, A. M. Caravaca-Aguirre, and R. Piestun, "Genetic algorithm optimization for focusing through turbid media in noisy environments," Opt. Express **20**, 4840–4849 (2012).
41. H. Wu, Z. Wang, M. Fan, L. Zhang, W. Zhang, and Y. Rao, "Role of the mirror's reflectivity in forward-pumped random fiber laser," Opt. Express **23**, 1421–1427 (2015).
42. S. Farahi, D. Ziegler, I. N. Papadopoulos, D. Psaltis, and C. Moser, "Dynamic bending compensation while focusing through a multimode fiber," Opt. Express **21**, 22504–22514 (2013).
43. Q. Feng, F. Yang, X. Xu, B. Zhang, Y. Ding, and Q. Liu, "Multi-objective optimization genetic algorithm for multi-point light focusing in wavefront shaping," Opt. Express **27**, 36459–36473 (2019).